What are the effects of environmental factors on Co speciation at magnetite surface?

Laura Fablet, Fadi Choueikani, Mathieu Pédrot, Rémi Marsac

View Article Online
View Journal

Environmental Science Nano

Accepted Manuscript

This article can be cited before page numbers have been issued, to do this please use: L. Fablet, F. Choueikani, M. Pédrot and R. Marsac, *Environ. Sci.: Nano*, 2024, DOI: 10.1039/D3EN00962A.

ROYAL SOCIETY OF CHEMISTRY

rsc.li/es-nano

View Article Online
DOI: 10.1039/D3EN00962A

Environmental significance

Magnetite nanoparticles are increasingly used and studied for the remediation of contaminated environments, due to their high affinity for metals, magnetic properties and natural presence in the environment. However, environmental factors such as pH, presence of natural organic molecules, and redox conditions have an impact on the stoichiometry of magnetite, and determine the adsorption of contaminants such as cobalt. Adsorption experiments and X-ray adsorption spectroscopy coupled with X-ray magnetic circular dichroism allowed to determine the amount and the speciation of Co bound to magnetite as a function of various environmental factors. The results of this work could help improve remediation using magnetite nanoparticles and better predict Co behavior in natural systems.

DOI: 10.1039/D3EN00962A

What are the effects of environmental factors on Co speciation at magnetite surface?

Laura Fablet[1,2], Fadi Choueikani[2], Mathieu Pédrot[1], and Rémi Marsac[1,3]*

[1] Univ Rennes, CNRS, Géosciences Rennes – UMR 6118, F-35000 Rennes, France

[2] Synchrotron SOLEIL, l'Orme des Merisiers, Départementale 128, 91190 Saint-Aubin, France

[3] Université Paris Cité, Institut de physique du globe de Paris, CNRS, F-75005 Paris, France

(*corresponding author: remi.marsac@cnrs.fr)

View Article Online
DOI: 10.1039/D3EN00962A

Abstract

Magnetite nanoparticles are abundant in the environment and are notably used for environmental applications due to their unique magnetic, adsorption and redox properties. The stoichiometry of magnetite (Fe(II)/Fe(III)) is dependent on environmental factors (pH, presence of organic ligands, redox conditions), which largely affects magnetite nanoparticles physico-chemical properties, such as redox reaction, but also adsorption of contaminants. However, the joint effects of environmental factors and magnetite stoichiometry on magnetite-metal cations interaction are elusive. This study focuses on Co as an important contaminant, and because Co-doped magnetite nanoparticles are of high interest for nanotechnology applications. Magnetite nanoparticles (~10nm) with different stoichiometries were synthesized by coprecipitation, and partially oxidized using H_2O_2 to obtain the desired stoichiometry. Batch studies were carried out with different [Co], using three different stoichiometries (0.1, 0.3 and 0.5), at different pH values, and in the presence or the absence of natural organic matter (OM) or atmospheric $O_{2(g)}$. Experimental and modeling results, and XAS and XMCD analysis revealed that interactions between Co and magnetite varied, with favored oligomer formation and surface precipitation at higher stoichiometries. It was also highlighted that the formation of different species of Co depended on environmental conditions with the adsorption of monomers favored at low pH and in the presence of organic matter, and the partial oxidation of Co(II) to Co(III) in aerobic conditions. These results will help to predict the behavior and fate of Co in the environment and to understand the impact of environmental factors for an appropriate use of magnetite nanoparticles for environmental applications, or to synthesize Co-modified magnetite nanoparticles using water as solvent for high technology applications.

1. Introduction

Iron (oxyhydr)oxide nanoparticle are ubiquitous and largely known to exert a strong control on the transport, speciation, (bio)availability, and biotoxicity of many contaminants in the environment though adsorption processes.[1–3] Contaminants interaction with iron (oxyhydr)oxide surfaces highly depends on physico-chemical factors such as pH, redox potential, ionic strength or the presence of organic coatings that can considerably vary between different natural systems. Interaction mechanisms between contaminants and iron (oxyhydr)oxides, and the effects of environmental factors on the extent of contaminants bound to the surface have been relatively well documented. This allowed, for instance, the development of mechanistic surface complexation models, that account for the impact of surface charging (related notably to surface protonation and background electrolyte concentration) to predict the chemical and electrostatic contribution to the ion surface complexation,[1,4] to account for polymer and surface precipitate formation,[5,6] the adsorption of Fe^{2+} and associated redox effects,[7,8] the formation of surface-metal-ligand ternary complexes with small organic or inorganic ligands,[9,10] as well as humic-like substances.[11–13] Although these surface speciation models are powerful tools to predict the behavior and fate of contaminants in naturals systems, further work is required to account for the impact of important adsorbing phases such as spinel iron oxide nanoparticles, including magnetite.

Spinel iron oxide nanoparticles ($Fe_{3-\delta}O_4$) are mixed compounds of Fe(II) and Fe(III), which occur naturally in the environment. Their structure is inverse with Fe(II) in the octahedral sites and Fe(III) in the octahedral and tetrahedral sites.[14–16] The full stoichiometric structure, which characterizes magnetite, is defined by a Fe(II)-to-Fe(III) ratio (R) equal to 0.5 (or $\delta = 0$).[17] Non-stoichiometric magnetite shows R values between 0 and 0.5 (or $0 \leqslant \delta \leqslant 1/3$). When R value tends to 0 ($\delta \rightarrow 1/3$), the magnetite structure is close to that of maghemite (Fe_2O_3), with the presence of iron vacancies in the octahedral sites and the absence of Fe(II).[17] The stoichiometry is dependent on various environmental factors, such as pH,[18] redox potential

(e.g. presence or absence of oxidants such as O_2 or H_2O_2 to reduce stoichiometry, or Fe^{2+} to restore stoichiometry),[17,19] microbial activity,[20] or organic ligands.[21,22] Thus, magnetites with different stoichiometries can exist in subsurface environments or in temporarily flooded soils, where conditions influence Fe valence.[23]

Besides the substantial changes in the magnetite structure imposed by the environmental conditions, and related changes in their electronic and magnetic properties,[3,24] magnetite stoichiometry also drastically affects its reactivity toward contaminants. The redox properties make magnetite very interesting for the reduction or oxidation of redox-sensitive chemical compounds at the magnetite surface in industrial and environmental processes,[19,25–30] or in medical applications.[31,32] Therefore, much effort has been made to characterize the impact of the stoichiometry on the thermodynamics and kinetics of the reduction reactions of inorganic and organic compounds, such as U(VI) reduction to U(IV)[26] or nitrobenzene reduction to aniline[19], or on its capacity to promote advanced oxidation processes trough Fenton-like reactions.[25,33] However, the impact of magnetite stoichiometry on surface complexation, polymerization and precipitation of metal ions have been largely overlooked. For instance, the adsorptions of several ligands (nalidixic acid, salicylate, and humic acid) were shown to increase with magnetite stoichiometry.[34] Similar observation was made by comparing the adsorption of Co^{2+} onto pristine and fully oxidized magnetite (i.e. maghemite).[35] However, available surface complexation models only consider pure magnetite or maghemite surfaces,[36,37] so the impact of magnetite stoichiometry on contaminants adsorption is not accurately predicted. By contrast with other iron (oxyhydr)oxide, the development of such model for magnetite is more challenging due to the dynamic behavior of the magnetite-maghemite solid solution. Further work is required to decouple the direct effects of environmental factors from the indirect ones, occurring through a modification of magnetite stoichiometry, on the surface speciation of metal ions such as Co^{2+}. This would, first, allow to better predict the impact of magnetite on their environmental behavior and fate, particularly in Fe-rich subsurface environments or temporary flooded soils (e.g., wetlands experiencing redox potential fluctuation). Second, as magnetite nanoparticles are widely used as adsorbents in water treatment due to various advantages (e.g. high adsorption capacity, easy magnetic separation from water, reusability, low toxicity and biocompatibility [38–42] a better prediction of magnetite adsorption capacity towards contaminants like Co might help optimizing its use in various physico-chemical conditions.

Predicting the surface speciation of Co is also interesting for the synthesis of nanomaterials for high technology applications. Indeed, surface-bound Co may improve the magnetic properties of magnetite nanoparticles, by decreasing their magnetic anisotropy at ambient temperature, while keeping a small size, which is of great interest for magneto-optic devices,[43,44] electronic devices,[45] data storage,[46–48] high-density recording[49] or even for replacing the rare earths contained in certain permanent magnets.[46,50] A previous study, evidenced the role of Co surface loading on Co speciation on stoichiometric magnetite,[51] which drastically affected the magnetic behavior of the nanoparticle. Surface complexed or incorporated Co^{2+} had a ferrimagnetic behavior at low loadings, magnetically-silent small Co polymers formed at intermediate loadings and precipitation of antiferromagnetic $Co(OH)_{2(s)}$-like phase onto the magnetite surface occurred for highest Co concentrations. Therefore, understanding the effects of physico-chemical parameters might allow to better constrain the properties of Co-modified magnetite nanoparticles.

The present study investigated the sorption of Co(II) on magnetite in aqueous suspensions, with the aim of unraveling the impacts of magnetite stoichiometry and important environmental factors (pH, organic ligands and oxidation) on the sorption and surface speciation of Co. Following a previous study on stoichiometric magnetite, adsorption isotherm experiments and modeling were performed and compared for non-stoichiometric magnetite, at pH 8 and under inert atmosphere, to avoid Fe^{2+} oxidation or H^+ promoted dissolution.[17,18] The effects of pH and humic acid concentration on both magnetite stoichiometry and Co(II) adsorption were

View Article Online
DOI: 10.1039/D3EN00962A

investigated under inert atmosphere, starting from a fully stoichiometric magnetite. Finally, the effect of O_2 on the redox speciation of Co at the surface of oxidized magnetite (quasi-maghemite) was also probed. All samples were characterized by X-ray absorption spectroscopy (XAS) and magnetic circular dichroism (XMCD) at Fe and Co $L_{2,3}$-edges. This allows to determine the oxidation state distribution of both elements (including magnetite stoichiometry),[17,18] their occurrence in octahedral or tetrahedral sites in spinel structure or at the surface of magnetite, and the surface speciation of Co, such as monomer, oligomer and $Co(OH)_2$-like phase formation.[51] The results provide important data for predicting Co speciation in the presence of magnetite in aqueous systems depending on environmental factors.

2. Materials and Methods

2.1. Chemicals

All chemicals used were purchased from Sigma-Adrich and were of analytical grade or better. Sample solutions were prepared with "MilliQ" ultrapure water (specific resistivity 18.2 MΩ cm). All the experiments, except the oxidation experiment, were performed in an anaerobic chamber (N_2-glovebox, JACOMEX, $O_{2(g)}$ < 1 ppm) and all the solutions were purged with $N_{2(g)}$ for at least 12 h inside the glovebox before use. The pH of all the samples were adjusted by HCl and NaOH (no buffer was used). For TEM measurements, hexadecyltrimethylammonium bromide (CTAB) was used as a surfactant. The Co hydroxide reference used was synthesized in a previous study.[51] The Co_3O_4 reference was purchased from Sigma-Adrich. Natural organic matter (OM) was purchased from the International Humic Substances Society (IHSS) and corresponded to the Leonardite humic acid (1S104H).

2.2. Synthesis of nanomagnetites with various stoichiometries

All syntheses were performed in an N_2-glovebox, at room temperature, following a well-known co-precipitation method of iron salts.[17,52,53] The full stoichiometric magnetite (R = Fe(II)/Fe(III) = 0.5) was synthesized with the dissolution of $FeCl_2$ and $FeCl_3$ in HCl solution, which was then added to NaOH solution leading to the instantaneous precipitation of ~10 nm magnetite nanoparticles. For non-stoichiometric nanoparticles (R = 0.1 and R = 0.3), known amounts of H_2O_2 were added to R0.5. The synthesized solutions were washed with ultrapure water (at pH ~ 8.5 to avoid the release of Fe^{2+}). The stoichiometry of the synthesized nanoparticles was verified by spectrophotometric determination of dissolved [Fe(II)] and total [Fe] (i.e., [Fe(III)] + [Fe(II)]) by the phenanthroline 1-10 colorimetric method.[54,55]

2.3. Sorption experiments

Aqueous suspensions of $Fe_{3-\delta}O_4$ nanoparticles (R0.1, R0.3, and R0.5) were prepared, for a total Fe concentration of 6.5 mM (~0.5 g L^{-1} of magnetite), in 15 mL tubes, with 10 mM NaCl. Isotherm experiments were performed at pH 8 and varying total Co concentration ($[Co]_{tot}$) from 0.01 to 3 mM (using a 100 mM $CoCl_2$ stock solution) for R0.1 and R0.3. Data for R0.5 were already obtained in a previous study.[51] The effects of pH were investigated using the three stoichiometries, for $[Co]_{tot}$ = 0.4 mM, and pH adjusted between 3 and 9. To understand the impact of OM, it was added to stoichiometric magnetite with concentrations ranging from 0 to 50 mg L^{-1}. Co was then added at a concentration of 0.04 mM and pH adjusted to 8. The concentrations of OM adsorbed on magnetites were measured by DOC (Dissolved Organic Carbon) analysis after sample filtration, by Shimadzu TOC-L carbon analyzer. To test the effect of oxidation on the Co adsorption process, a sample was prepared from R0.1 with $[Co]_{tot}$ = 3 mM, and the pH was adjusted to 8, in aerobic conditions. $N_{2(g)}$ bubbling was used to limit

carbonate dissolution. After 7 days of equilibrium, a magnet was used to collect the solid fraction of all the samples. The supernatant was filtered at 0.2 µm using cellulose PES filters (Sartorius Minisart). Cobalt concentrations were determined using a UV-Vis spectrophotometric method, adapted from Zahir and Keshtkar (1998).[51,55–57] It is based on a complexation of Co^{2+} with 1-Nitroso-2-naphthol-3,6-disulfonic acid disodium salt hydrate (nitroso-R salt). The absorbance was recorded at 520 nm with a Shimadzu UV2600 spectrophotometer. A cobalt calibration curve was determined, with concentrations ranging from between 5 to 100 µM, for the quantification of aqueous Co concentration in the filtered solutions ($[Co]_{aq}$). For the samples with very small $[Co]_{aq}$ (i.e. < 5 µM), a quadrupole ICP-MS (Agilent Technologies 7700X) was used. Before Co quantification, calibration curves were performed and validated using certified material references (SLRS-6, National Research Council). A rhodium solution was used as an internal standard to correct the instrumental drift and potential matrix effects. The limit of Co quantification was determined at 18 nM (1.04 ppt) (AFNOR Certification).[58] The total amount of Co associated with the solid phase was expressed in term of Co surface density onto $Fe_{3-\delta}O_4$ ($[Co]_s$, in atom nm^{-2}) and calculated as follows:

$$[Co]_s = ([Co]_{tot} - [Co]_{aq}) * \frac{V}{m} * \frac{1}{SSA} * N_A * 10^{-18} (1)$$

where $[Co]_{tot}$ and $[Co]_{aq}$ are given in mol L^{-1}, V is the sample volume (L), m is the magnetite mass (g), SSA is the surface specific area (m^2 g^{-1}) and N_A is the Avogadro constant (mol^{-1}). On the basis of repetition of some experiments, uncertainty associated with Co adsorption was 5%.

A cobalt ferrite suspension was prepared by following the magnetite synthesis method (see section 2.2), replacing 10% of the Fe(II) ($FeCl_2.4H_2O$) with Co(II) ($CoCl_2.6H_2O$), in a N_2 glovebox, at room temperature. NaOH was added until pH was stable at 8.5 and the solution was kept as is.

2.4. Characterization by TEM

Different nanoparticles samples were characterized by transmission electron microscopy (HR-TEM; Jeol JEM 2100 HR microscope). A small volume of sample was taken (Co-magnetite, Co-OM-magnetite), which was then diluted with ultrapure water. All samples were sonicated for 15 min. A droplet of the diluted suspension was deposited on a Holey carbon film 300 mesh copper grid and dried inside the anaerobic chamber, except for the oxidized sample, which was made under aerobic conditions. Samples were transported to the microscope in hermetically sealed glass bottles, preserving them under a N_2 atmosphere. The average particle diameter of the pristine magnetite was found equal to 11.5 ± 1.5 nm for R0.5, 10.6 ± 2.6 nm for R0.3 and 9.6 ± 2.6 nm for R0.1, by measuring 100 particles.[17,18]

2.5. XAS and XMCD analyses

Solid samples were analyzed by XAS and XMCD, covering the soft X-ray range and probing the $L_{2,3}$ range (2p → 3d) absorption edges of Fe and Co transition metals. XAS and XMCD analyses, which are chemically selective and sensitive to valence states, were helping to better understand the contribution of Co and Fe cations to the structure and magnetic behavior of nanoparticles. XAS and XMCD spectra were recorded on the DEIMOS beamline at synchrotron SOLEIL.[59] Measurements were carried out on dried nanoparticles, by dropping colloidal suspensions on silicon plates which were dried at room temperature in an Ar-glove box (JACOMEX $O_{2(g)}$ < 1 ppm) connected to the DEIMOS station. The silicon plates were fixed to a copper sample holder, which was then introduced into the superconducting magnet of

DEIMOS end station. All the spectra were collected in total electron yield (TEY) at 4.2 K and in UHV conditions (10^{-10} mbar). XAS spectra were recorded by reversing the full circular polarization of the X-rays to the right (σ_R) or left (σ_L), and by varying the external magnetic field (H = +6 or -6 T). Isotropic XAS spectra were plotted as $(\sigma^+ + \sigma^-)/2$, while the XMCD results were plotted as $(\sigma^+ - \sigma^-)$, where $\sigma^+ = [\sigma_L(H^-) + \sigma_R(H^+)]/2$ and $\sigma^- = [\sigma_L(H^+) + \sigma_R(H^-)]/2$. For all the Co spectra, the background of XAS and XMCD at the Co $L_{2,3}$ edges were corrected by subtracting from the raw signal the XAS and XMCD results of the corresponding pure magnetite (R0.1, R0.3 or R0.5, without Co) sample measured at Co edges. Then, XAS and XMCD were normalized by dividing the raw signal by the edge jump of the isotropic XAS. By measuring XMCD intensity as a function of external magnetic fields (from +6 to -6T), XMCD magnetization curves at specific sites on the Co L_3 edge of Co were plotted. At DEIMOS beamline, the fully circularly polarized X-rays were provided by an Apple-II HU52 undulator for XAS and XMCD, while EMPHU65 with a polarization flipping rate of 10 Hz was used to record the magnetization curves. The beam size was 800 × 800 μm2 and the photon energy resolution was 100 meV.

The different peaks obtained by Fe XMCD at L_3-edge were used to estimate the stoichiometry of the samples. The evolution of peak intensities were be monitored using the S indicator:[17,60]

$$S = \frac{(S_1 + S_2)}{(S_2 + S_3)} \qquad (2)$$

The peak S_1 is attributed to Fe(II) and Fe(III) in octahedral sites, although Fe(II) dominates. The S_2 peak corresponds to Fe(III) in tetrahedral sites, while the S_3 peak corresponds to the contribution of Fe(III) in octahedral sites.[17] The S indicator was then used to calculate the effective stoichiometry according to the method described in Jungcharoen et *al.* (2021).[17]

3. Results and Discussion

3.1. Effect of magnetite stoichiometry on Co adsorption

Co adsorption as a function of their concentrations was studied on three different stoichiometries: R0.1, R0.3 and R0.5. TEM images are shown in Fig. S2 for the two extreme Co concentrations ($[Co]_s$ = 0.5; 18.9 and 25.7 atom nm^{-2} respectively) for R0.1 and R0.5. The Co adsorption isotherms measured for the three stoichiometries, at pH 8, are shown in Fig 1, using linear scales, and in Fig. S3 using log scales that allow to visualize Co sorption behavior at trace levels, relevant to natural systems (data in Table S1). Data for R0.5 were taken from our previous study.[51] The evolution of the data as a function of Co concentration reveals three steps with (i) a large amount of Co adsorbed at low concentration, (ii) a change of slope with more Co in solution at intermediate concentration and (iii) a linear adsorption at high Co concentration. At low Co surface loadings (< 0.1 nm^{-2}), adsorption is similar and strong for all three stoichiometries because Co either forms monomeric surface complexes or incorporates into the $Fe_{3-\delta}O_4$ surface structure.[35,51] As Co loading increases, adsorption on R0.1 shows a plateau at around 4 nm^{-2}, compared with 10 nm^{-2} for R0.3 and R0.5. A previous study dedicated to Co adsorption on magnetite at pH 8, but under oxidizing conditions, observed an adsorption plateau between 1.25 and 3.45 atom nm^{-2}, depending on the surface area of the magnetite.[56] As the surface of these magnetites was very likely oxidized under ambient atmosphere, the adsorption data compare well with the present ones obtained for R0.1.[56] At such loadings, Co was shown to form small polymers on R0.5.[51] This implies that, by contrast with monomeric Co species, surface polynuclear Co species formation is affected by the stoichiometry of magnetite. Similar observation was made with an organic ligand (nalidixic acid), for which the adsorption increased from 0 to 100% at pH 8 when the stoichiometry increased.[34] Above the plateau, as the Co concentration in solution increases, the amount of Co in the solid phase rises non-linearly for $[Co]_{aq}$ > 0.2 mM for R0.3 and R0.5, and $[Co]_{aq}$ > 0.6

mM for R0.1. This Co behavior can be attributed to Co surface precipitation. The fact that the onset of Co surface precipitation is found at larger $[Co]_{aq}$ suggests that the surface of R0.1 serves less efficiently as a template for Co-(hydr)oxide precipitation than higher stoichiometry magnetites. This observation is consistent with the smaller capacity of R0.1 to promote the formation of polynuclear Co species, compared to R0.3 and R0.5, because the latter species might be regarded as a first step before further polymerization process.

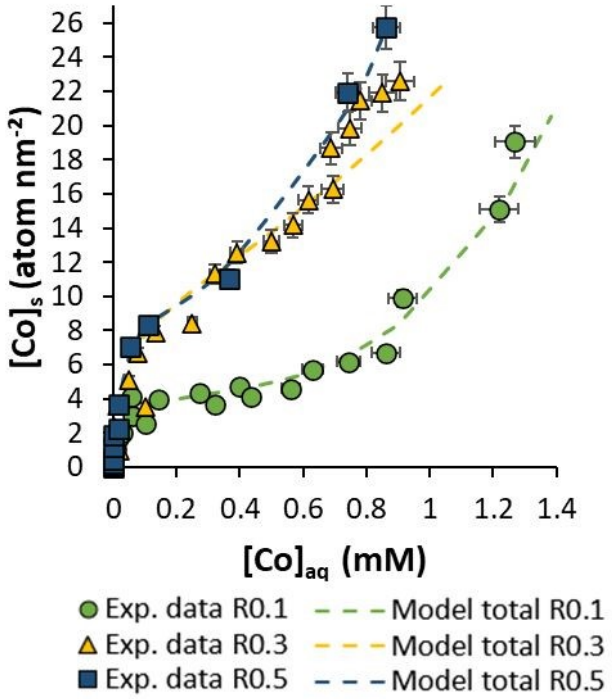

Fig. 1 *Cobalt adsorption isotherms on R0.1 and R0.3 (6.5 mM Fe) at pH 8, in 10 mM NaCl. Symbols represent the experimental data ("Exp. data"). The dotted lines correspond to the model results, which is a combination of two Langmuir and one Freundlich models. Results are compared with data obtained for R0.5, taken from Fablet et al.*, 2023.[51] Analytical error bars of 5% are plotted, although not visible for some data and at logarithmic scale. Error was set to 50% for data with $[Co]_{aq}$ < 0.001 mM on the logarithmic scale (i.e. ± 0.2 log unit)[61] to acknowledge the fact that larger error may be encountered at low concentrations.

The experimental data are compared with model results obtained by the combination of the two Langmuir and Freundlich adsorption isotherm equations, with the following equations, as described in a previous study and applied to R0.5:[51]

$$[Co]_s = Q_{L,1} + Q_{L,2} + Q_F \quad (3)$$

where $Q_{L,i}$ (i = 1 or 2) and Q_F are magnetite-bound Co amounts. The eqn (4) described $Q_{L,i}$:

$$Q_{L,i} = Q_{max,i}\frac{K_{L,i}[Co]_{aq}}{1 + K_{L,i}[Co]_{aq}} \quad (4)$$

where $Q_{max,i}$ is the adsorption capacity (here, in atom per nm²) and $K_{L,i}$ is the Langmuir constant (in L mmol^{-1}). And the eqn (3) described Q_F:

$$Q_F = K_F[Co]_{aq}^n \quad (5)$$

where K_F is the Freundlich constant, and n is the non-ideality parameter.

Results of the fit are shown in Fig. 1, for $[Co]_s$, and the contributions of the three considered mechanisms on the overall adsorption are shown in Fig. S3. The equation 3-5 parameters for each stoichiometry are shown in Table 1. Preliminary tests revealed that K_{L1} and K_{L2} values were similar for all stoichiometries, and were subsequently constrained equal in order to follow only the evolution of $Q_{max,i}$, K_F and n. Although the first Langmuir equation seems negligible at a linear scale, it appears crucial to predict Co behavior at naturally relevant trace levels, which are visualized using log scales (Fig. S3). The first adsorption mechanism, at low Co concentrations where surface complexation of Co-monomers is expected to be the prevalent mechanism, is similar for the three different stoichiometries, with a $Q_{max,1}$ = 0.52 atom nm^{-2} and log K_{L1} = 4.18. The second mechanism differ for R0.1, R0.3 and R0.5, with $Q_{max,L2}$ values equal to 4.16, 9.48 and 10.51 atom nm^{-2} respectively. Finally, the third mechanism, which used the Freundlich equation to account for surface precipitation (as it can be seen as a multi-layer formation)[62–64] also differs between the three stoichiometries, with n-K_F couples leading to a onset of $Co(OH)_2$ precipitation at $[Co]_{aq}$ = 0.4 mM for R0.1, and approximately 0.1 mM for R0.3 and R0.5. This difference in Co behavior could be explained by the fact that R0.1 magnetite, which has a structure close to that of maghemite, has less Fe on its surface, replaced by vacancies, which might limit Co-oligomers and precipitate formation on its surface. As already pointed out,[51] the present model is simple and cannot be considered as a predictive model of Co interaction with magnetite, because it does not include electrostatic contribution to the surface Co-magnetite binding, for instance. However, the model is used as a semi-quantitative guide for interpreting isotherm and spectroscopic data by accounting for three distinct surface species.

;***Table 1*** *Optimized parameters of equation 3, for Langmuir models (L_1 and L_2) and Freundlich model (F), for R0.1, R0.3 and R0.5. Q_{max} is the adsorption capacity (atom nm^{-2}).*

Stoichiometry	Parameters	L_1	L_2	F
R0.1	n			3.27
	Log K	4.18	1.39	0.34
	Q_{max}	0.52	4.16	
R0.3	n			1.43
	Log K	4.18	1.39	0
	Q_{max}	0.52	9.48	
R0.5	n			2.41
	Log K	4.18	1.39	0.25
	Q_{max}	0.52	10.51	

The speciation of $Fe_{3-\delta}O_4$-bound Co as a function of its stoichiometry was investigated at several Co concentrations by XAS and XMCD analysis. All isotropic XAS and XMCD spectra at the Co L_3-edge are presented in Fig. S4. Selected results obtained for the three

stoichiometries at three different $[Co]_s$, for which each surface species determined by the surface speciation model prevail are shown in Fig. 2 ($[Co]_{tot}$ = 0.04, 0.2 and 3 mM, corresponding to $[Co]_s$ = 0.5, 2-2.3 and 18.9-25.7 atom nm^{-2}, respectively). The XAS spectra show four contributions at approximately 772.1 eV (peak A), 773.4 eV (peak B), 773.8 eV (peak C), and 774.7 eV (peak D), which are the multiplet peaks characteristic of the presence of Co^{2+} (Fig. 2a, b and c).[65] All XAS spectra were normalized to the C peak in order to study the evolution of the other peaks. The XAS spectra of the samples show few differences at low (Fig. 2a) and medium (Fig. 2b) Co concentrations, which are similar to the reference spectrum of $CoFe_2O_4$ (Fig. S1) or that of adsorbed Co organic complexes to magnetite.[66,67] Large A and D peaks at high Co concentrations (Fig. 2c), as observed for $Co(OH)_2$ (reference taken from Fablet *et al.*, 2023),[51] point to the formation of $Co(OH)_2$-like phase on the surface of all the magnetites. However, slightly more intense A and D peaks observed for R0.1 might suggest a larger extent of $Co(OH)_2$ formation. XMCD spectra provide complementary information to XAS spectra and exhibit two peaks E (773.5 eV) and F (773.9 eV) (Fig. 2d, e and e). For low and intermediate Co concentrations (e.g. $[Co]_{tot}$ = 0.04 and 0.2 mM, Fig. 2d, e), the XMCD spectra of all stoichiometries resemble either to the $CoFe_2O_4$ reference spectrum or to the spectrum of adsorbed Co complexes to magnetite.[46,66,67] At high Co concentrations (e.g. $[Co]_{tot}$ = 3 mM in Fig. 2f), the XMCD spectra of the samples resembles that of $Co(OH)_2$, which is characterized by a smaller peak E (as probed by the E/F peak ratio in Fig. S5) that is slightly shifted to lower energy. Hence, XMCD results also confirm surface precipitation at high $[Co]_{tot}$ for all magnetites.

View Article Online
DOI: 10.1039/D3EN00962A

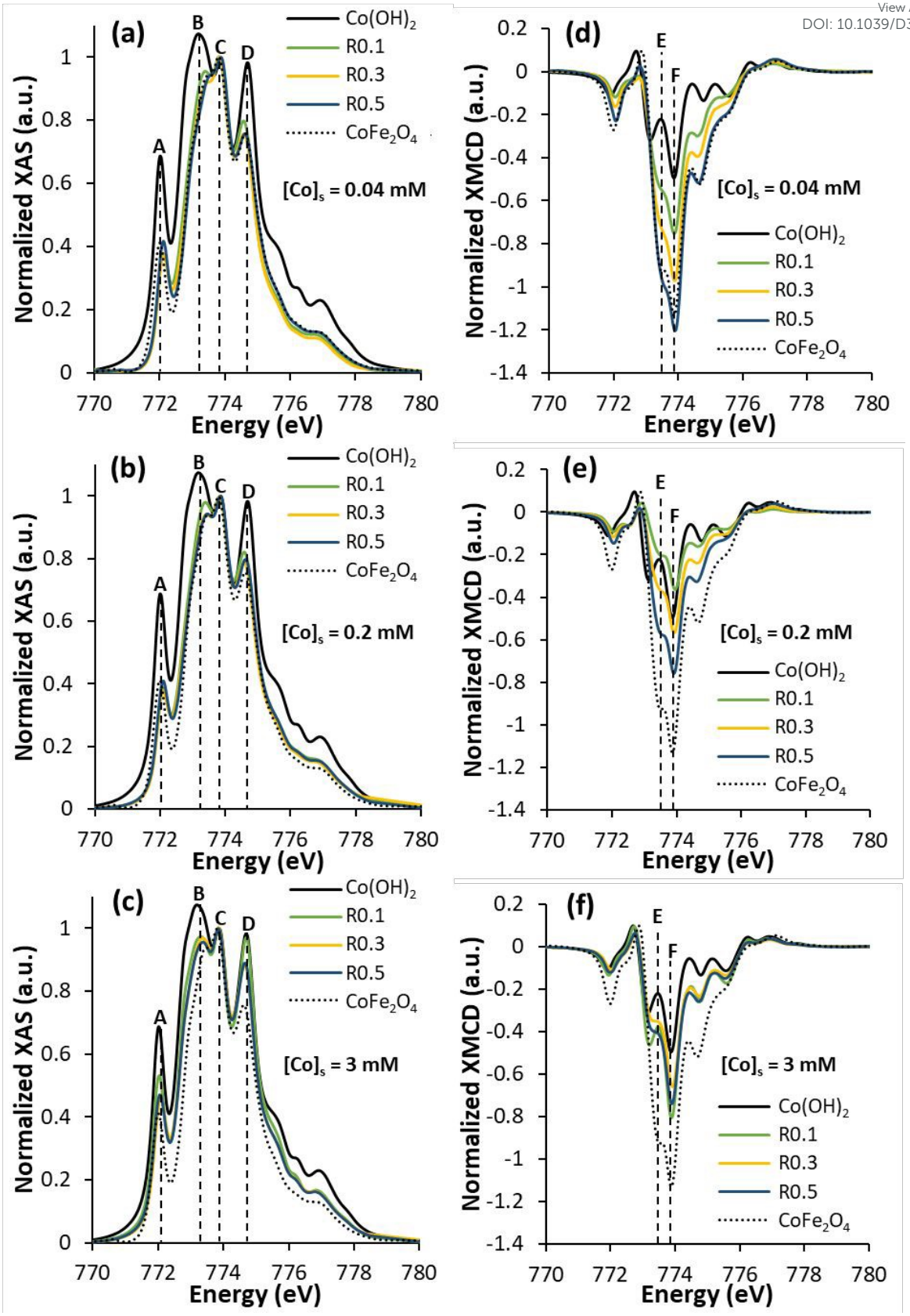

Fig. 2 *Normalized XAS spectra at the Co L_3-edge at (a) $[Co]_{tot}$ = 0.04 mM, (b) $[Co]_{tot}$ = 0.2 mM, and (c) $[Co]_{tot}$ = 3 mM, and normalized XMCD spectra at the Co L_3-edge at (d) $[Co]_{tot}$ = 0.04 mM, (e) $[Co]_{tot}$ = 0.2 mM, and (f) $[Co]_{tot}$ = 3 mM, for the three magnetite stoichiometries: R0.1 in green, R0.3 in yellow, and R0.5 in blue (data for R0.5 from Fablet et al., 2023).[51] The dotted line corresponds to the XAS and XMCD of $CoFe_2O_4$ and the solid line to $Co(OH)_2$ references. XAS signals are normalized by dividing the raw signal by the maximum XAS peak, and XMCD signals are normalized by dividing the raw signal by the maximum XAS peak.*

View Article Online
DOI: 10.1039/D3EN00962A

Important variations in the intensity of the XMCD signal are observed depending on R and $[Co]_{tot}$. The largest signal is observed for R0.5 at low $[Co]_{tot}$ (Fig. 2d), and was attributed to Co adsorption in the form of a monomer, whose structure is close to that of a ferrimagnetic $CoFe_2O_4$ structure.[51] At low and intermediate [Co] (Fig. 2d,e), that is, in the absence of $Co(OH)_2$ precipitation, the XMCD signal decreases with decreasing R, which is probably due to smaller magnetic Fe-Co coupling for non-stoichiometric than for stoichiometric magnetites. By contrast the XMCD signal is only little affected by R for high $[Co]_{tot}$ (Fig. 2f), which confirms that $Co(OH)_2$ prevails at the surface of all stoichiometries. As previously observed for R0.5, XAS and XMCD spectra at the Fe $L_{2,3}$ edge show no significant effect of Co on Fe solid speciation (Fig. S6).[17]

The XMCD signal intensity is plotted against $[Co]_{tot}$ for each stoichiometry in Fig. 3, and is compared with the predicted surface speciation of Co calculated with the isotherm model (eqn. 1). For all three magnetite stoichiometries, the decrease in the XMCD signal seems to be linked to the decrease in the first species (i.e. Co monomers) and the formation of the second species (i.e. Co oligomers). Moreover, the XMCD signal increases when the models predict $Co(OH)_2$ formation. These results confirm previous observation that XMCD can be used to probe Co speciation at the surface of magnetite.[51] These data were also compared with the results of linear combination fit (LCF), on normalized Co L_3-edge XAS spectra for each stoichiometry (from 770 to 780 eV) to determine the percentage of $Co(OH)_2$ versus the Co surface loading, used with the $CoFe_2O_4$ and $Co(OH)_2$ references (Fig. S7, Table S2).[51] The results obtained agree qualitatively with those of surface modeling on the increase in the amount of $Co(OH)_2$. This is because linear combinations of XAS do not allow differentiation of the second species, Co oligomers, as shown for R0.5 magnetite.[51]

View Article Online
DOI: 10.1039/D3EN00962A

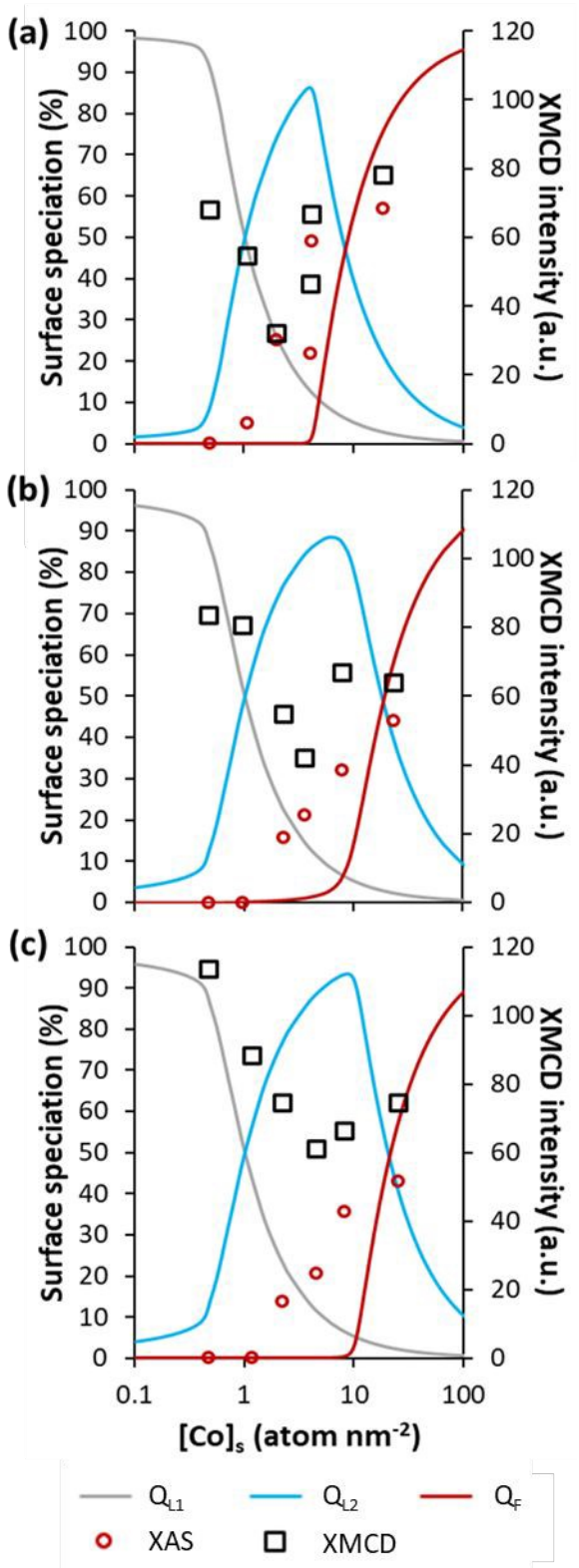

Fig. 3 *Percentage of the different species identified using the adsorption eqn (1) versus Co surface loading in log scale (in atom nm^{-2}) compared to the percentage of the Co(OH)$_{2(s)}$-like phase calculated from LCF of XAS data (red circles) and, on the secondary axis, the XMCD intensity (black squares), for (a) R0.1, (b) R0.3 and (c) R0.5 (data for R0.5 from Fablet et al., 2023).*[51]

The XMCD magnetization curves versus the magnetic field at $Co^{2+}_{(Oh)}$ site for R0.1, R0.3 and R0.5 with $[Co]_{tot}$ = 0.8 mM are shown on Fig. 4. The magnetic properties depend on the valence states of the elements and the alignment of cation moments in the crystal structure. Thus, the high-field saturation provides confirmation on the sorption behavior of Co on the surface of the

various stoichiometry. For R0.5 the magnetization curve tends to a saturation at high magnetic field which is in great agreement with a ferrimagnetic structure similar to $CoFe_2O_4$. However, decreasing the stoichiometry the magnetization curves tends to the non saturation at high field. Especially for R0.1, the magnetization curve shows no saturation, similarly to the one of $Co(OH)_2$, which exhibits an antiferromagnetic structure. This is due to a larger proportion of $Co(OH)_2$ on R0.1, compared to R0.3 and R0.5, which limits saturation.

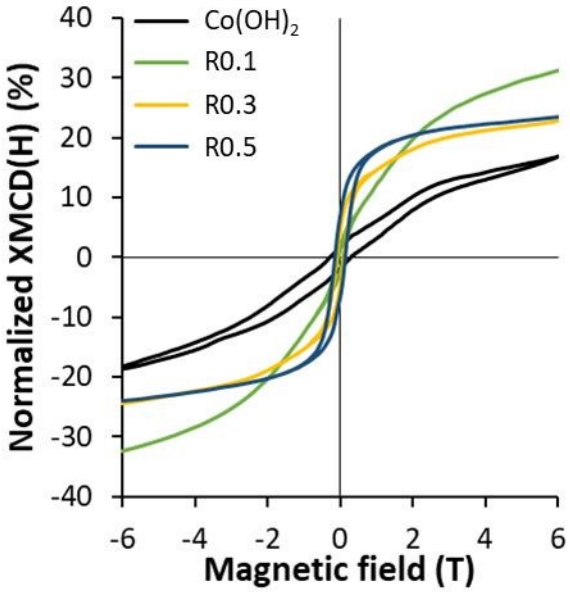

Fig. 4 *Normalized XMCD magnetization in percentage versus magnetic field measurement at Co L_3-edge at 4.2 K for $[Co]_s$ = 4.16, 7.88 and 8.30 atom nm^{-2} for R0.1, R0.3 and R0.5 respectively (corresponding to $[Co]_{tot}$ = 0.8 mM), and for $Co(OH)_2$. Spectra are plotted as 2*(CR – CL)/(CR + CL), with CR is the spectrum of polarization circular right and CL the spectrum of polarization circular left.*

3.2. Effect of pH on Co adsorption onto magnetites

To get insights into the stability of Co-oligomers *versus* monomers, the effect of pH on Co adsorption was investigated for intermediate $[Co]_{tot}$ (0.4 mM, where Co-oligomers occur at pH 8), over a pH range from 3 to 10 for R0.1 and R0.5 (Fig. 5a). For the two stoichiometries the effect of pH on cobalt adsorption is similar, with almost no adsorption at pH values below 5, followed by an increase in adsorbed amount up to a complete Co removal from the solution at pH 8. However, slightly larger Co adsorption at 6.5 ≤ pH ≤ 8 onto R0.5 than onto R0.1. XAS and XMCD spectra at the Fe and Co $L_{2,3}$-edges were recorded for R0.5 at pH = 6.5, pH at which $[Co]_s$ = 2 atoms nm^{-2} (~40% adsorbed). According to the Fe data (Fig. S8), no significant change in magnetite stoichiometry was observed between pH 6.5 and 8 (R_{eff} = 0.48 and 0.53 ± 0.05, respectively).[17] The XAS spectra of Co show no clear differences between the two pH values (Fig. S9). However, the XMCD spectrum (Fig. 5b) recorded at pH 6.5 shows an intense F peak and exhibits similar features to $CoFe_2O_4$, by contrast with the less intense signal and a spectrum that resembles $Co(OH)_2$ at pH 8. This difference is due to the smaller amount of Co adsorbed on the magnetite surface at pH 6.5 than at pH 8, which favors the formation of surface Co monomeric species. In addition, oligomer formation and surface precipitation reactions of metal ions onto Fe-(hydro)oxides generally involve a larger stoichiometric number of OH^- and, hence, only occur at relatively high pH values, by contrast with monomeric surface complexation that can occur at comparatively lower pH values.[11] Finally, because (i) magnetite surface charge evolves with pH,[36,37] and (ii) surface Co-oligomers and monomers might not carry the same charge, electrostatic effects can be expected to play a combined role with pH on the Co surface speciation.

View Article Online
DOI: 10.1039/D3EN00962A

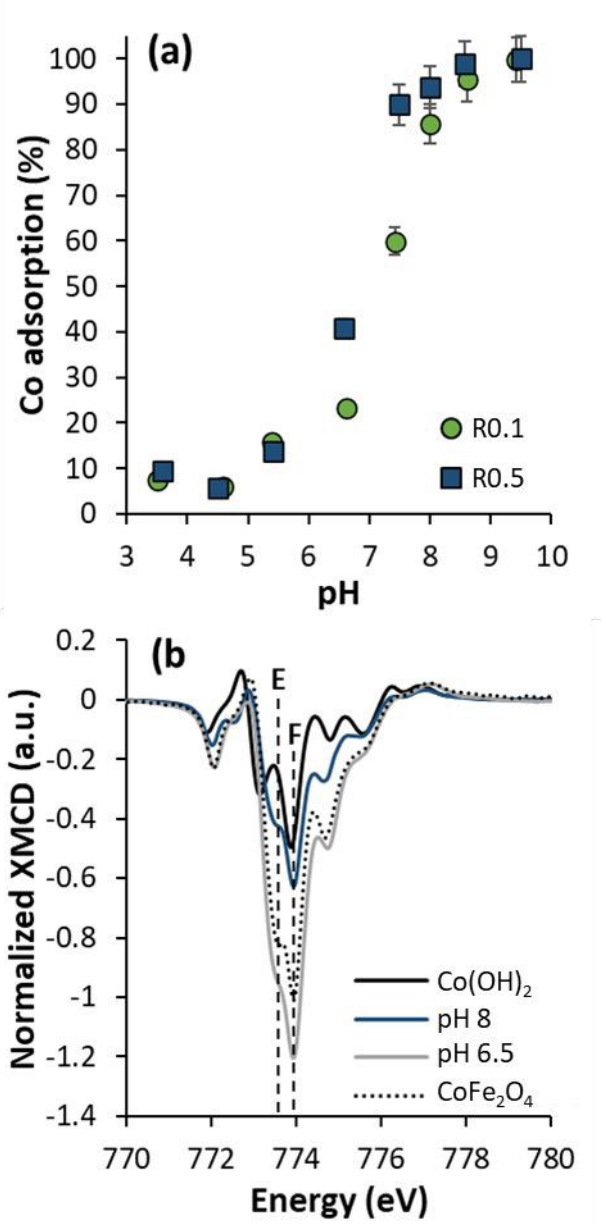

Fig. 5 *(a) Effect of pH on the percentage of Co adsorbed for two stoichiometry of magnetite: R0.1 (green circles), and R0.5 (blue squares), for $[Co]_{tot}$ = 0.4 mM, and (b) corresponding normalized XMCD spectra at the Co L_3-edge at pH 6.5 (gray line) and 8 (blue line) for stoichiometric magnetite (R0.5). The dotted line corresponds to the XMCD of $CoFe_2O_4$ and the solid line to $Co(OH)_2$ references. XMCD signals are normalized by dividing the raw signal by the maximum XAS peak.*

3.3. Organic matter (OM) effects on Co adsorption on stoichiometric magnetite (R0.5)

The effects of OM on Co surface complexation onto stoichiometric magnetite was studied for low $[Co]_{tot}$ (0.04 mM, where Co monomers prevail) with OM concentrations ranging from 2 to 50 mg L^{-1}, at pH 8. Magnetite and OM were pre-equilibrated before the addition of Co in order to maximize the effects of OM on Co surface speciation. Fig. 6a compares the percentage of adsorbed Co and the OM concentration in solid phase in mgC g^{-1} versus the total OM concentration. Adsorbed OM increases with total concentration, with over 90% of OM adsorbed for [OM] ≤ 10 mg L^{-1}, but with a low slop, suggesting surface site saturation at high [OM], with only 59% of OM adsorbed for [OM] = 50 mg L^{-1}. The percentage of Co adsorbed is only little affected by OM for [OM] ≤ 25 mg L^{-1}, as it remains between 95 and 90%. This can be either due to the strong interaction between Co and magnetite, or ternary complexes (FeO-Co-L or Fe-L-Co) often formed in the presence of different ligands (L), including natural organic

View Article Online
DOI: 10.1039/D3EN00962A

matter.[11,13,66,67] For [OM] = 50 mg L^{-1}, Co adsorption decreases to 46%.[68,69] XAS and XMCD analyses at the Fe $L_{2,3}$-edge (Fig. S11a, c) revealed that MO dissolves magnetite by preferential adsorption with Fe(II), inducing a more oxidized surface of the magnetite. However, because magnetite stoichiometry (R) decreases from 0.48 to 0.42, for 2 ≤ [OM] ≤ 25 mg L^{-1}, and decreases to 0.32 when [OM] = 50 mg L^{-1}, this cannot explain alone the decrease in Co adsorption but, instead, this can be attributed to solution complexation between Co and OM.[70,71] It is interesting to note that, while TEM images for [OM] = 2 mg L^{-1} show no significant effect of OM on magnetite nanoparticles aggregation, for [OM] = 50 mg L^{-1}, very small Fe nanoparticles (around 2 nm-sized) appear. These small nanoparticles might arise from the released Fe(II) under the influence of OM and subsequent oxidation to Fe(III). Fe(III) nanoparticles formed from Fe(II)-OM complexes are known to exhibit very small sizes.[72,73]

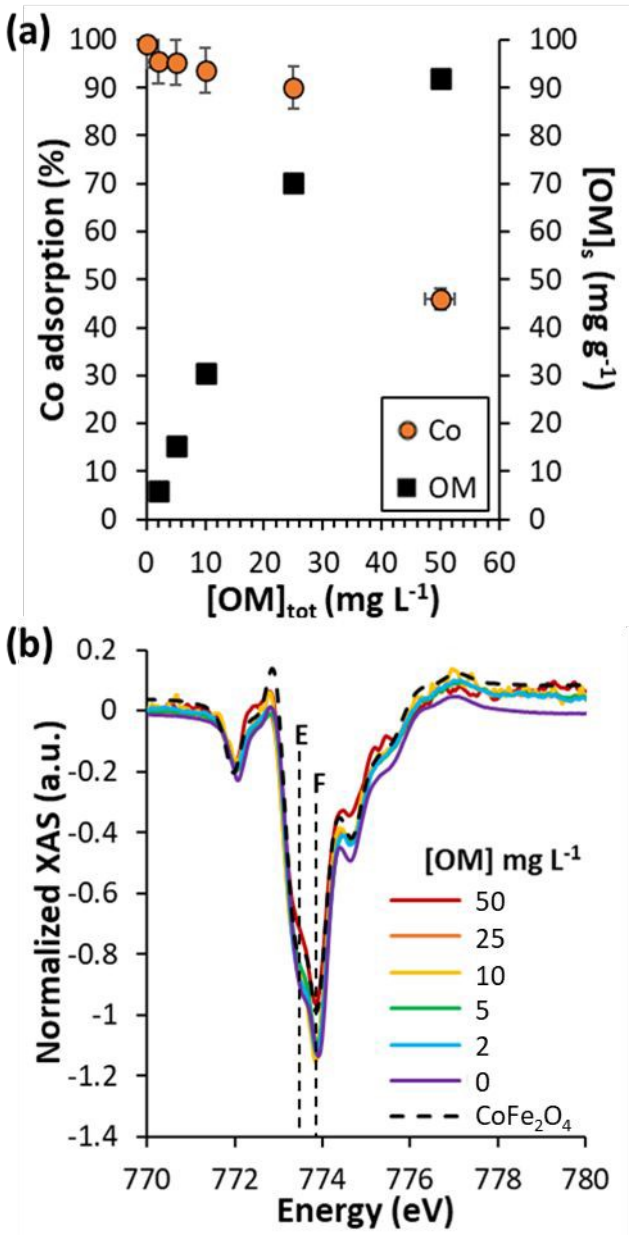

Fig. 6 *(a) Adsorption of organic matter (OM) in mg g^{-1} Fe_3O_4 (black squares) and percentage of adsorbed cobalt (orange circles) and (b) XMCD at the Co L_3-edge on stoichiometric magnetite (R0.5) (6.5 mM Fe), at pH 8, for $[OM]_{tot}$ = 2 to 50 mg L^{-1} and $[Co]_{tot}$ = 0.04 mM. XMCD of Co signals are normalized by dividing the raw signal by the maximum XAS peak.*

The XAS (Fig. S11b) and XMCD (Fig. 6b) spectra of Co are similar for all [OM], except for [OM] = 50 mg L^{-1}, which has a slightly less intense XMCD signal. It is recalled that the intensity

of the XMCD signal cannot be related to the smaller amount of Co adsorbed at high [OM] (see e.g. Fig. 4 and related discussions). Instead this might be due to the binding of Co at the outer shell of a thick layer of OM, which can only weakly interact magnetically with the particle, as previously observed when the particle was covered with a layer of an organic molecule.[74]

3.4. Oxidation effects on Co adsorption on R0.1 magnetite

Redox conditions, especially the occurrence of $O_{2(g)}$ might also have an impact on Co interaction with magnetite. Indeed, TEM images (Fig. S12) reveal that R0.1 equilibrated with $[Co]_{tot}$ = 3 mM under aerobic conditions at pH 8 is highly aggregated, with the formation of some leaflet structures. No evolution of magnetite stoichiometry was observed from Fe XAS and XMCD spectra because the already oxidized magnetite R0.1 was used. Adsorption measurements showed that in aerobic conditions, 7.1 atom nm^{-2} were associated with magnetite, compared with 19.9 atom nm^{-2} in anaerobic conditions, which points to a different Co speciation in the absence or presence of O_2. The corresponding Co XAS spectrum (Fig. 7a) shows a small peak A and a very intense peak at 775.3 eV (denoted G). It shares common characteristics with the XAS spectrum of Co_3O_4, a mixed compound of Co(II) and Co(III), which has no peak A, and a very intense peak G, characteristic of Co(III). Corresponding XMCD spectra are shown in Fig. 7b. Co_3O_4 has no signal, being an antiferromagnetic material. A XMCD signal is measured for the sample in aerobic condition, although weaker than that of the sample stored in anaerobic condition, which evidences the co-occurence of Co(II) magnetically coupled to magnetite. Furthermore, the XMCD spectrum of the oxidized sample is similar to the spectrum of $CoFe_2O_4$, by contrast with the sample prepared in the absence of O_2, which has a shape similar to that of $Co(OH)_2$. Previous studies have shown that Co(II) rapidly oxidized to Co(III) at room temperature, forming a Co_3O_4 phase on the particle surface.[70,71] Total oxidation of Co to Co_3O_4 can be limited by the presence of CoO on the outermost layers.[70,75] XAS and XMCD results suggest that, under aerobic conditions, partial oxidation of Co(II) to Co(III) limits $Co(OH)_2$ precipitation in favor of Co(II) monomers and a Co_3O_4-like precipitate.

View Article Online
DOI: 10.1039/D3EN00962A

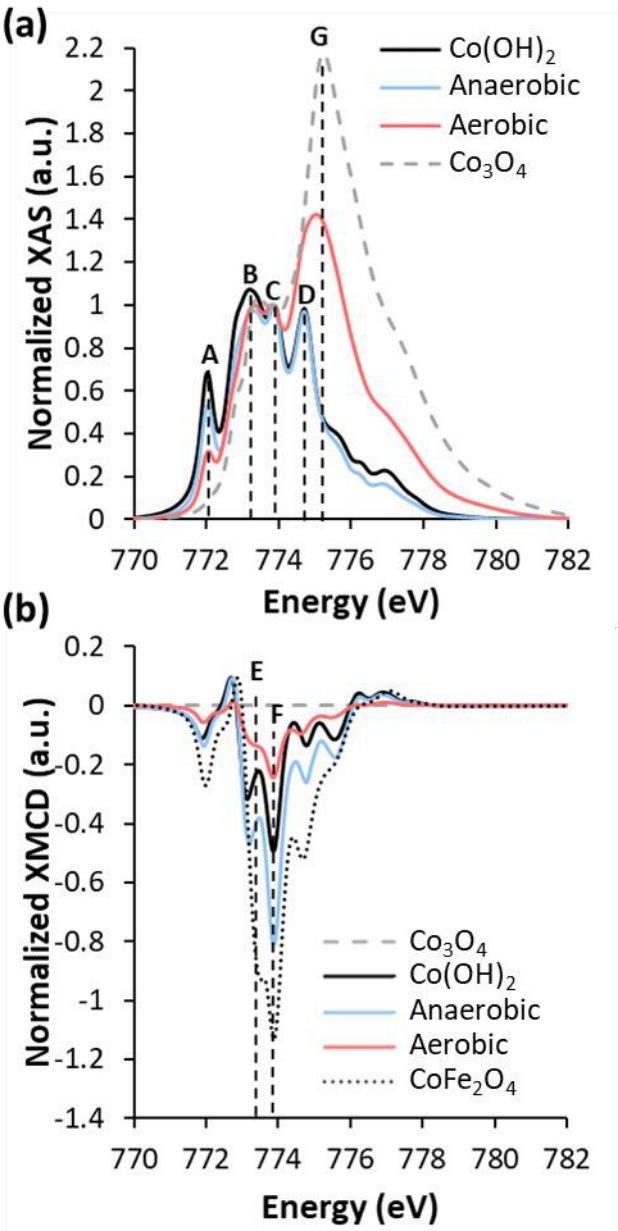

Fig. 7 *Normalized XAS (a) and (b) XMCD spectra at the Co L_2-edge, of non-stoichiometric magnetite (R0.1) in anaerobic conditions (blue), with $[Co]_s$ = 19.9 atom nm^{-2}, and aerobic conditions (red), with $[Co]_s$ = 7.1 atom nm^{-2} ($[Fe]_{tot}$ = 6.5 mM and $[Co]_{tot}$ = 3mM; pH 8), with references of $Co(OH)_2$ (black line), Co_3O_4 (dashed gray line) and $CoFe_2O_4$ (dotted black line). XAS and XMCD of Co signals are normalized by dividing the raw signal by the XAS peak C.*

4. Conclusions

Magnetite nanoparticles are increasingly being studied for environmental applications, due to their unique properties and natural presence in the environment. Their affinity with metals and their easy synthesis make them ideal candidates for water and soil remediation. However, the adsorption of metals onto magnetite is highly dependent on environmental factors. This study is focused on the interactions between Co and nanomagnetite as a function of magnetite stoichiometry (Fe(II)/Fe(III) = 0.1, 0.3 and 0.5), pH, the presence of organic matter and redox conditions. The impact of various environmental factors was probed by adsorption experiments and XAS and XMCD analyses. The results show that magnetite stoichiometry plays a crucial role in Co adsorption, which depended on Co surface loading. While no

important effects are observed at trace Co levels, where monomers in ferrimagnetic structure prevail, non-stoichiometric magnetite had smaller capacity to promote the formation of magnetically-silent polynuclear Co species, and appeared to serve less efficiently as a template for antiferromagnetic Co-(hydr)oxide precipitation than higher stoichiometry magnetites. In addition, results revealed a significant impact of the other environmental factors studied, with Co adsorption limited to acid pH and monomers adsorption favored due to both competition with H^+ for magnetite surface sites and the larger stoichiometric number of H^+ involved in cation polymerization reaction. Co adsorption was little affected by [OM], unless very large concentrations were tested ([OM] = 50 mg L^{-1}), which might be due to the formation of ternary complexes between surface sites, Co and OM. Nevertheless, Co^{2+} remained magnetically interacting with magnetite at all [OM]. Finally, partial oxidation of Co(II) to Co(III) occurred on the magnetite surface under aerobic conditions, hence limiting the formation of $Co(OH)_2$-like in favor of a Co_3O_4-like phase. This study has shed light onto the joint effects of magnetite stoichiometry and environmental factors on Co adsorption, surface speciation and magnetic behavior on magnetite surface. Present data might also be used for the development of a mechanistic surface complexation model that should not only account for the various phenomena listed in above in the introduction (e.g. surface charging and related electrostatic effects, competition with cations and protons, ternary complexes with inorganic ligands and OM), but also the indirect effects - through a modification of magnetite stoichiometry - of pH, redox conditions, and OM on Co(II) adsorption to magnetite. Indeed, as magnetite stoichiometry is strongly correlated with pH and redox conditions, knowledge of Co speciation as a function of magnetite stoichiometry and environmental factors is essential for better control remediation from magnetite nanoparticles, to predict environmental mechanisms, and potentially for the synthesis of Co-modified magnetite nanoparticles using water as solvent.

Author contributions

Laura Fablet: writing-original draft, data curation, investigation, visualization. Mathieu Pédrot: writing – review & editing, resources, supervision, project administration, funding acquisition. Fadi Choueikani: writing – review & editing, resources, supervision, project administration, funding acquisition. Anthony Beauvois: writing – review & editing. Rémi Marsac: writing – review & editing, resources, supervision, project administration, funding acquisition.

Conflicts of interest

There are no conflicts to declare.

Acknowledgments

This work was supported by the French Brittany Region (ARED project “NANOMAG”), SOLEIL synchrotron, the “COLOSSAL” project funded by ANR (project number ANR-23-CE01-0001) and the SURFNANO project funded by the CNRS-INSU EC2CO program. Through the support of the GeOHeLiS analytical platform of Rennes University, this publication is also supported by the European Union through the European Regional Development Fund (FEDER), the French Ministry of Higher Education and Research, the French Region of Brittany and Rennes Metropole. The authors further acknowledge the SOLEIL synchrotron for beamtime allocation at the DEIMOS beamline (proposal no. 20210864). The authors are grateful to M. Bouhnik-Le Coz and M. Pattier for assistance in ICP-MS and UV-vis analysis, V. Dorcet and L. Rault for assistance in TEM experiments performed on the THEMIS platform (ScanMAT, UMS 2011 University of Rennes-CNRS; CPER-FEDER 2007–2014), as well as M. Pasturel (Institute of Chemical Sciences of Rennes) for assistance in XRD analysis

References

1 D. A. Dzombak and F. M. M. Morel, *Surface Complexation Modeling: Hydrous Ferric Oxide*, John Wiley & Sons, New York, 1991.

2 M. Ponthieu, F. Juillot, T. Hiemstra, W. H. van Riemsdijk and M. F. Benedetti, Metal ion binding to iron oxides, *Geochim. Cosmochim. Acta*, 2006, **70**, 2679–2698.

3 R. M. Cornell and U. Schwertmann, *The Iron Oxides: Structure, Properties, Reactions, Occurences and Uses*, Wiley-VCH: Berlin, 1st edn., 2003.

4 T. Hiemstra and W. H. Van Riemsdijk, A Surface Structural Approach to Ion Adsorption: The Charge Distribution (CD) Model, *J. Colloid Interface Sci.*, 1996, **179**, 488–508.

5 I. M. Ugwu and D. M. Sherman, Irreversibility of sorption of cobalt to goethite (α-FeOOH) and disparities in dissolution of aged synthetic Co-goethite, *Chem. Geol.*, 2017, **467**, 168–176.

6 J. Lutzenkirchen and Ph. Behra, On the surface precipitation model for cation sorption at the (hydr)oxide water interface, *Aquat. Geochem.*, 1996, **1**, 375–397.

7 T. Hiemstra and W. H. van Riemsdijk, Adsorption and surface oxidation of Fe(II) on metal (hydr)oxides, *Geochim. Cosmochim. Acta*, 2007, **71**, 5913–5933.

8 W. Cheng, J. Li, J. Sun, T. Luo, R. Marsac, J.-F. Boily and K. Hanna, Nalidixic Acid and Fe(II)/Cu(II) Coadsorption at Goethite and Akaganéite Surfaces, *Environ. Sci. Technol.*, 2023, **57**, 15680–15692.

9 W. Cheng, E. L. Kalahroodi, R. Marsac and K. Hanna, Adsorption of Quinolone Antibiotics to Goethite under Seawater Conditions: Application of a Surface Complexation Model, *Environ. Sci. Technol.*, 2019, **53**, 1130–1138.

10 L. Zhou, W. Cheng, R. Marsac, J.-F. Boily and K. Hanna, Silicate surface coverage controls quinolone transport in saturated porous media, *J. Colloid Interface Sci.*, 2022, **607**, 347–356.

11 L. Weng, W. H. Van Riemsdijk and T. Hiemstra, Cu2+ and Ca2+adsorption to goethite in the presence of fulvic acids, *Geochim. Cosmochim. Acta*, 2008, **72**, 5857–5870.

12 J. Li, L. Weng, Y. Deng, J. Ma, Y. Chen and Y. Li, NOM-mineral interaction: Significance for speciation of cations and anions, *Sci. Total Environ.*, 2022, **820**, 153259.

13 P. E. Reiller, Modelling metal–humic substances–surface systems: reasons for success, failure and possible routes for peace of mind, *Mineral. Mag.*, 2012, **76**, 2643–2658.

14 C. A. Gorski and M. M. Scherer, Influence of Magnetite Stoichiometry on FeII Uptake and Nitrobenzene Reduction, *Environ. Sci. Technol.*, 2009, **43**, 3675–3680.

15 G. F. Goya, T. S. Berquó, F. C. Fonseca and M. P. Morales, Static and dynamic magnetic properties of spherical magnetite nanoparticles, *J. Appl. Phys.*, 2003, **94**, 3520–3528.

16 B. Issa, I. M. Obaidat, B. A. Albiss and Y. Haik, Magnetic Nanoparticles: Surface Effects and Properties Related to Biomedicine Applications, *Int. J. Mol. Sci.*, 2013, **14**, 21266–21305.

17 P. Jungcharoen, M. Pédrot, F. Choueikani, M. Pasturel, K. Hanna, F. Heberling, M. Tesfa and R. Marsac, Probing the effects of redox conditions and dissolved Fe 2+ on nanomagnetite stoichiometry by wet chemistry, XRD, XAS and XMCD, *Environ. Sci.: Nano*, 2021, **8**, 2098–2107.

18 P. Jungcharoen, M. Pédrot, F. Heberling, K. Hanna, F. Choueikani, C. Catrouillet, A. Dia and R. Marsac, Prediction of nanomagnetite stoichiometry (Fe(II)/Fe(III)) under contrasting pH and redox conditions, *Environ. Sci.: Nano*, 2022, **9**, 2363–2371.

19 C. A. Gorski, J. Nurmi, P. Tratnyek, T. Hofstetter and M. M. Scherer, Redox Behavior of Magnetite: Implications for Contaminant Reduction, *Environ. Sci. Technol.*, 2010, **44**, 55–60.
20 J. M. Byrne, N. Klueglein, C. Pearce, K. M. Rosso, E. Appel and A. Kappler, Redox cycling of Fe(II) and Fe(III) in magnetite by Fe-metabolizing bacteria, *Science*, 2015, **347**, 1473–1476.
21 P. Jungcharoen, R. Marsac, F. Choueikani, D. Masson and M. Pédrot, Influence of organic ligands on the stoichiometry of magnetite nanoparticles, *Nanoscale Adv.*, 2023, **5**, 4213–4223.
22 A. Sundman, J. M. Byrne, I. Bauer, N. Menguy and A. Kappler, Interactions between magnetite and humic substances: redox reactions and dissolution processes, *Geochem. Trans.*, 2017, **18**, 6.
23 B. A. Maher and R. M. Taylor, Formation of ultrafine-grained magnetite in soils, *Nature*, 1988, **336**, 368–370.
24 W. Kündig and R. Steven Hargrove, Electron hopping in magnetite, *Solid State Commun.*, 1969, **7**, 223–227.
25 M. Usman, J. M. Byrne, A. Chaudhary, S. Orsetti, K. Hanna, C. Ruby, A. Kappler and S. B. Haderlein, Magnetite and Green Rust: Synthesis, Properties, and Environmental Applications of Mixed-Valent Iron Minerals, *Chem. Rev.*, 2018, **118**, 3251–3304.
26 D. E. Latta, C. A. Gorski, M. I. Boyanov, E. J. O'Loughlin, K. M. Kemner and M. M. Scherer, Influence of Magnetite Stoichiometry on UVI Reduction, *Environ. Sci. Technol.*, 2012, **46**, 778–786.
27 C.-H. Liu, Y.-H. Chuang, T.-Y. Chen, Y. Tian, H. Li, M.-K. Wang and W. Zhang, Mechanism of Arsenic Adsorption on Magnetite Nanoparticles from Water: Thermodynamic and Spectroscopic Studies, *Environ. Sci. Technol.*, 2015, **49**, 7726–7734.
28 M. L. Peterson, A. F. White, Brown Gordon E. and G. A. Parks, Surface Passivation of Magnetite by Reaction with Aqueous Cr(VI): XAFS and TEM Results, *Environ. Sci. Technol.*, 1997, **31**, 1573–1576.
29 Z. Pan, B. Bártová, T. LaGrange, S. M. Butorin, N. C. Hyatt, M. C. Stennett, K. O. Kvashnina and R. Bernier-Latmani, Nanoscale mechanism of UO2 formation through uranium reduction by magnetite - à lire, *Nat Commun*, 2020, **11**, 4001.
30 L. Gao, J. Zhuang, L. Nie, J. Zhang, Y. Zhang, G. Ning, T. Wang, J. Feng, D. Yang, S. Perrett and X. Yan, Intrinsic peroxidase-like activity of ferromagnetic nanoparticles, *Nature nanotechnology*, 2007, **2**, 577–83.
31 R. A. Revia and M. Zhang, Magnetite nanoparticles for cancer diagnosis, treatment, and treatment monitoring: recent advances, *Mater. Today*, 2016, **19**, 157–168.
32 Z. R. Stephen, F. M. Kievit and M. Zhang, Magnetite nanoparticles for medical MR imaging, *Mater. Today*, 2011, **14**, 330–338.
33 S. G. Ardo, S. Nélieu, G. Ona-Nguema, G. Delarue, J. Brest, E. Pironin and G. Morin, Oxidative Degradation of Nalidixic Acid by Nano-magnetite via Fe2+/O2-Mediated Reactions, *Environ. Sci. Technol.*, 2015, **49**, 4506–4514.
34 W. Cheng, R. Marsac and K. Hanna, Influence of Magnetite Stoichiometry on the Binding of Emerging Organic Contaminants, *Environ. Sci. Technol.*, 2018, **52**, 467–473.
35 A. Uheida, G. Salazar-Alvarez, E. Björkman, Z. Yu and M. Muhammed, Fe3O4 and γ-Fe2O3 nanoparticles for the adsorption of Co2+ from aqueous solution, *J. Colloid Interface Sci.*, 2006, **298**, 501–507.

36 R. Jolsterå, L. Gunneriusson and A. Holmgren, Surface complexation modeling of Fe3O4–H+ and Mg(II) sorption onto maghemite and magnetite, *Journal of Colloid and Interface Science*, 2012, **386**, 260–267.
37 N. Morelová, N. Finck, J. Lützenkirchen, D. Schild, K. Dardenne and H. Geckeis, Sorption of americium / europium onto magnetite under saline conditions: Batch experiments, surface complexation modelling and X-ray absorption spectroscopy study, *J. Colloid Interface Sci.*, 2020, **561**, 708–718.
38 S. C. N. Tang and I. M. C. Lo, Magnetic nanoparticles: Essential factors for sustainable environmental applications, *Water Research*, 2013, **47**, 2613–2632.
39 L. Carlos, F. S. G. Einschlag, M. C. González, D. O. Mártire, L. Carlos, F. S. G. Einschlag, M. C. González and D. O. Mártire, in *Waste Water - Treatment Technologies and Recent Analytical Developments*, IntechOpen, 2013.
40 M. Namdeo, Magnetite Nanoparticles as Effective Adsorbent for Water Purification-A Review, *Advances in Recycling & Waste Management*, 2017, **2**, 1–13.
41 Y.-M. Hao, C. Man and Z.-B. Hu, Effective removal of Cu (II) ions from aqueous solution by amino-functionalized magnetic nanoparticles, *Journal of Hazardous Materials*, 2010, **184**, 392–399.
42 J. Hu, G. Chen and I. M. C. Lo, Removal and recovery of Cr(VI) from wastewater by maghemite nanoparticles, *Water Research*, 2005, **39**, 4528–4536.
43 F. Choueikani, F. Royer, D. Jamon, A. Siblini, J. J. Rousseau, S. Neveu and J. Charara, Magneto-optical waveguides made of cobalt ferrite nanoparticles embedded in silica/zirconia organic-inorganic matrix, *Appl. Phys. Lett.*, 2009, **94**, 051113.
44 H. Amata, F. Royer, F. Choueikani, D. Jamon, F. Parsy, J.-E. Broquin, S. Neveu and J. Jacques Rousseau, Hybrid magneto-optical mode converter made with a magnetic nanoparticles-doped SiO2/ZrO2 layer coated on an ion-exchanged glass waveguide, *Appl. Phys. Lett.*, 2011, **99**, 251108.
45 M. Sugimoto, The Past, Present, and Future of Ferrites, *J. Am. Chem. Soc.*, 1999, **82**, 269–280.
46 K. Sartori, G. Cotin, C. Bouillet, V. Halté, S. Bégin-Colin, F. Choueikani and B. P. Pichon, Strong interfacial coupling through exchange interactions in soft/hard core–shell nanoparticles as a function of cationic distribution, *Nanoscale*, 2019, **11**, 12946–12958.
47 S. Staniland, W. Williams, N. Telling, G. Laan, A. Harrison and B. Ward, Controlled cobalt doping of magnetosomes in vivo, *Nature nanotechnology*, 2008, **3**, 158–62.
48 B. Babukutty, N. Kalarikkal and S. S. Nair, Studies on structural, optical and magnetic properties of cobalt substituted magnetite fluids (CoxFe1−xFe2O4), *Mater. Res. Express*, 2017, **4**, 035906.
49 S. P. Gubin, Y. I. Spichkin, G. Y. Yurkov and A. M. Tishin, Nanomaterial for High-Density Magnetic Data Storage, *Russ. J. Inorg. Chem.*, 2002, **47**, 32–67.
50 F. Choueikani, D. Jamon, S. Neveu, M.-F. Blanc-Mignon, Y. Lefkir and F. Royer, Self-biased magneto-optical films based on CoFe2O4–silica nanocomposite, *Journal of Applied Physics*, 2021, **129**, 023101.
51 L. Fablet, F. Choueikani, M. Pédrot, M. Kerdiles, M. Pasturel and R. Marsac, Investigation of magnetite–Co interactions: from environmentally relevant trace Co levels to core–shell Fe3O4@Co(OH)2 nanoparticles with magnetic applications, *Environ. Sci.: Nano*, , DOI:10.1039/D3EN00379E.
52 R. Massart, Preparation of aqueous magnetic liquids in alkaline and acidic media, *IEEE Trans. Magn.*, 1981, **17**, 1247–1248.

53 E. Demangeat, M. Pédrot, A. Dia, M. Bouhnik-le-Coz, F. Grasset, K. Hanna, M. Kamagate and F. Cabello-Hurtado, Colloidal and chemical stabilities of iron oxide nanoparticles in aqueous solutions: the interplay of structural, chemical and environmental drivers, *Environ. Sci.: Nano*, 2018, **5**, 992–1001.
54 W. B. Fortune and M. G. Mellon, Determination of Iron with o-Phenanthroline: A Spectrophotometric Study, *Ind. Eng. Chem. Anal. Ed.*, 1938, **10**, 60–64.
55 H. Tamura, N. Katayama and R. Furuichi, The Co2+Adsorption Properties of Al2O3, Fe2O3, Fe3O4, TiO2, and MnO2Evaluated by Modeling with the Frumkin Isotherm, *J. Colloid Interface Sci.*, 1997, **195**, 192–202.
56 A. Motl, F. Šebesta, J. D. Navratil and J. Hlavicova, Sorption of cobalt on magnetite, *Czechoslov. J. Phys.*, 2003, **53**, A515–A523.
57 R. Marsac, M. Pasturel and K. Hanna, Reduction Kinetics of Nitroaromatic Compounds by Titanium-Substituted Magnetite, *J. Phys. Chem. C*, 2017, **121**, 11399–11406.
58 D. Yeghicheyan, D. Aubert, M. Bouhnik-Le Coz, J. Chmeleff, S. Delpoux, I. Djouraev, G. Granier, F. Lacan, J.-L. Piro, T. Rousseau, C. Cloquet, A. Marquet, C. Menniti, C. Pradoux, R. Freydier, E. Vieira da Silva-Filho and K. Suchorski, A New Interlaboratory Characterisation of Silicon, Rare Earth Elements and Twenty-Two Other Trace Element Concentrations in the Natural River Water Certified Reference Material SLRS-6 (NRC-CNRC), *Geostand. Geoanalytical Res.*, 2019, **43**, 475–496.
59 P. Ohresser, E. Otero, F. Choueikani, K. Chen, S. Stanescu, F. Deschamps, T. Moreno, F. Polack, B. Lagarde, J.-P. Daguerre, F. Marteau, F. Scheurer, L. Joly, J.-P. Kappler, B. Muller, O. Bunau and Ph. Sainctavit, DEIMOS: A beamline dedicated to dichroism measurements in the 350–2500 eV energy range, *Rev. Sci. Instrum.*, 2014, **85**, 013106.
60 S. Brice-Profeta, M.-A. Arrio, E. Tronc, N. Menguy, I. Letard, C. Cartier dit Moulin, M. Noguès, C. Chanéac, J.-P. Jolivet and Ph. Sainctavit, Magnetic order in γ-Fe2O3 nanoparticles: a XMCD study, *J. Magn. Magn. Mater.*, 2005, **288**, 354–365.
61 M. H. Bradbury and B. Baeyens, Sorption modelling on illite. Part II: Actinide sorption and linear free energy relationships, *Geochimica et Cosmochimica Acta*, 2009, **73**, 1004–1013.
62 K. J. Farley, D. A. Dzombak and F. M. M. Morel, A surface precipitation model for the sorption of cations on metal oxides, *Journal of Colloid and Interface Science*, 1985, **106**, 226–242.
63 M. R. Matsumoto, P. M. McGinley, B. E. Reed and J. N. Jensen, Physicochemical Processes, *Water Environment Research*, 1992, **64**, 337–346.
64 J.-S. Kwon, S.-T. Yun, J.-H. Lee, S.-O. Kim and H. Y. Jo, Removal of divalent heavy metals (Cd, Cu, Pb, and Zn) and arsenic(III) from aqueous solutions using scoria: Kinetics and equilibria of sorption, *Journal of Hazardous Materials*, 2010, **174**, 307–313.
65 M. W. Haverkort, Thesis, University Koeln, 2005.
66 Y. Prado, N. Daffé, A. Michel, T. Georgelin, N. Yaacoub, J.-M. Grenèche, F. Choueikani, E. Otero, P. Ohresser, M.-A. Arrio, C. Cartier-dit-Moulin, P. Sainctavit, B. Fleury, V. Dupuis, L. Lisnard and J. Fresnais, Enhancing the magnetic anisotropy of maghemite nanoparticles via the surface coordination of molecular complexes, *Nat. Commun.*, 2015, **6**, 1–8.
67 V. E. Campbell, M. Tonelli, I. Cimatti, J.-B. Moussy, L. Tortech, Y. J. Dappe, E. Rivière, R. Guillot, S. Delprat, R. Mattana, P. Seneor, P. Ohresser, F. Choueikani, E. Otero, F. Koprowiak, V. G. Chilkuri, N. Suaud, N. Guihéry, A. Galtayries, F. Miserque, M.-A. Arrio, P. Sainctavit and T. Mallah, Engineering the magnetic coupling and anisotropy at the

molecule–magnetic surface interface in molecular spintronic devices, *Nat. Commun.*, 2016, **7**, 13646.

68 I. Christl and R. Kretzschmar, Interaction of copper and fulvic acid at the hematite-water interface, *Geochim. Cosmochim. Acta*, 2001, **65**, 3435–3442.

69 S. Masset, F. Monteil-Rivera, L. Dupont, J. Dumonceau and M. Aplincourt, Influence of humic acid on sorption of Co(II), Sr(II), and Se(IV) on goethite, *Agronomie*, 2000, **20**, 525–535.

70 V. Papaefthimiou, T. Dintzer, V. Dupuis, A. Tamion, F. Tournus, A. Hillion, D. Teschner, M. Hävecker, A. Knop-Gericke, R. Schlögl and S. Zafeiratos, Nontrivial Redox Behavior of Nanosized Cobalt: New Insights from Ambient Pressure X-ray Photoelectron and Absorption Spectroscopies, *ACS Nano*, 2011, **5**, 2182–2190.

71 H. Singh, Thesis, Homi Bhabha National Institute, 2015.

72 D. Vantelon, M. Davranche, R. Marsac, C. L. Fontaine, H. Guénet, J. Jestin, G. Campaore, A. Beauvois and V. Briois, Iron speciation in iron–organic matter nanoaggregates: a kinetic approach coupling Quick-EXAFS and MCR-ALS chemometrics, *Environ. Sci.: Nano*, 2019, **6**, 2641–2651.

73 H. Guénet, M. Davranche, D. Vantelon, J. Gigault, S. Prévost, O. Taché, S. Jaksch, M. Pédrot, V. Dorcet, A. Boutier and J. Jestin, Characterization of iron–organic matter nano-aggregate networks through a combination of SAXS/SANS and XAS analyses: impact on As binding, *Environ. Sci.: Nano*, 2017, **4**, 938–954.

74 Y.-J. Hsu, Y.-L. Lai, C.-H. Chen, Y.-C. Lin, H.-Y. Chien, J.-H. Wang, T.-N. Lam, Y.-L. Chan, D. H. Wei, H.-J. Lin and C.-T. Chen, Enhanced Magnetic Anisotropy via Quasi-Molecular Magnet at Organic-Ferromagnetic Contact, *J. Phys. Chem. Lett.*, 2013, **4**, 310–316.

75 S. Zafeiratos, T. Dintzer, D. Teschner, R. Blume, M. Hävecker, A. Knop-Gericke and R. Schlögl, Methanol oxidation over model cobalt catalysts: Influence of the cobalt oxidation state on the reactivity, *J. Catal.*, 2010, **269**, 309–317.